Biophysical Journal, Volume *119*

Supplemental Information

Differential Diffusional Properties in Loose and Tight Docking Prior to Membrane Fusion

Agata Witkowska, Susann Spindler, Reza Gholami Mahmoodabadi, Vahid Sandoghdar, and Reinhard Jahn

Image background correction using image registration

For image background (BG) correction we developed a routine which we call Sparse In Time Affine Registration (SITAR).The procedure is briefly described in the following: Each frame is divided into 16 equally-sized boxes with 3-pixel overlap between all neighboring boxes. For each box, a stack of images (usually 25 with a spacing of 30 frames) is aligned by translation and scaling to register the images to the frame of interest (also called "affine mapping"). An optimization routine is applied to find the coefficients of the registered group of images to optimally describe the background of the frame of interest in this region. Finally, each pixel value in the box is divided by the estimated background value and multiplied by the mean value of the background box. The image is recomposed from the BG-corrected boxes without the overlapping regions.

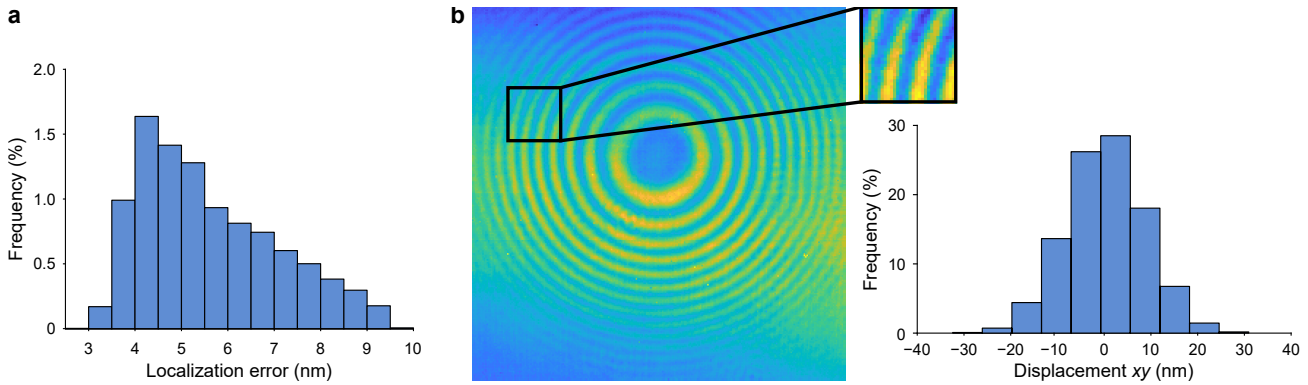

Figure S1 Localization accuracy of determined LUV localization. (a) Localization error distribution for *x* and *y* directions of the trajectory shown in Fig. 2a. Bin width 0.5 nm. All positions with a fit error larger than 0.15 pixel size (corresponding to 9.54 nm) were neglected. (b) Determination of translational GUV dynamics. A GUV region (indicated in the snapshot) is selected to calculate the displacement of the same region relative to the GUV recorded 2 ms earlier in the video. Histogram presents displacements of such GUV translation. Color map encodes iSCAT gray values. Bin width = 6.3 nm; standard deviation = 8.

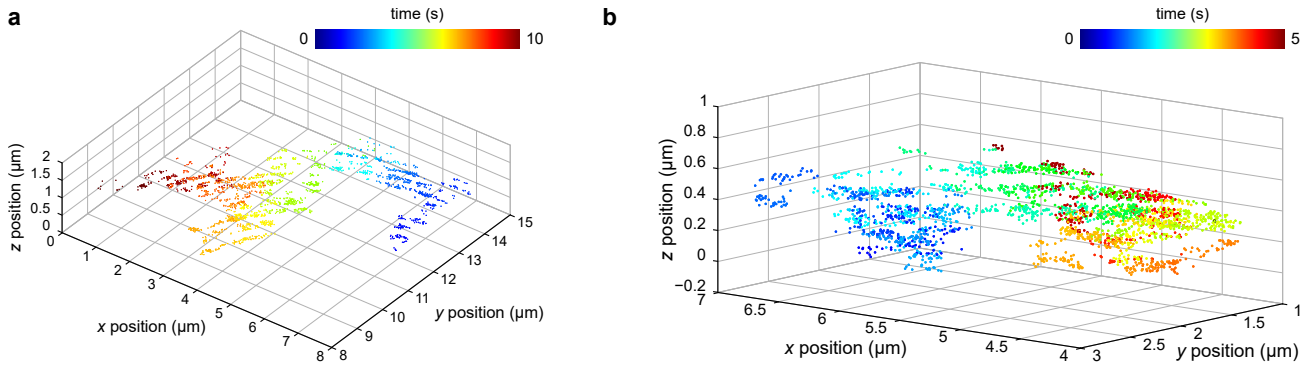

Figure S2 3D reconstructed trajectories of a docked liposomes. Localizations of Δ84 syb- (a) and WT syb- (b) liposomes docked on the GUV surface and tracked for 10 s (a) and 5 s (b), respectively. Point color encodes for the time evolution (see also Fig. 2a).

Determining the GUV center

To find the coarse and more accurate position of the GUV center (x_{GUV}, y_{GUV}), we applied two consecutive routines. For the coarse determination of the GUV center, the direction perpendicular to the fringes in small image segments was computed. To do so, the raw iSCAT image was divided into 16 segments and each segment was thresholded individually as shown in Fig. S3a. The Fourier transform of each binary segment (Fig. S3b) was approximated by an ellipse using image moments. The major axis of the ellipse was directed along the frequencies with high intensity and thus towards the GUV center. The eccentricity of the ellipse gives a measure for the strength of the directionality. Hence, a vector could be assigned to each segment with the direction along the major ellipse axis and the eccentricity as length (Fig. S3c). The intersection of all vectors determines the coarse GUV center with an accuracy on the order of a few pixels (1), depending on the number and quality of the GUV rings, which can in turn be affected by illumination inhomogeneities or strong scatterers in the field of view.

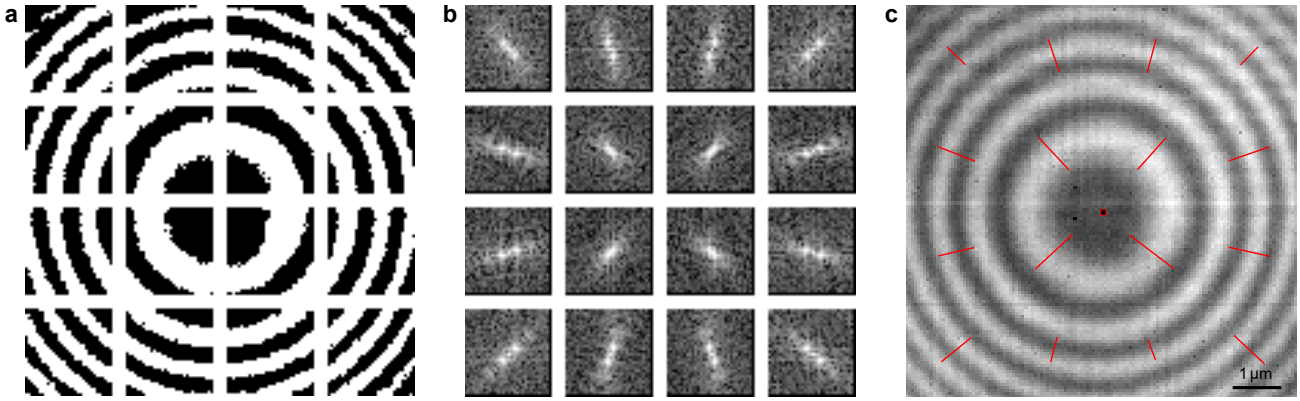

Figure S3 Coarse determination of the GUV center position from its iSCAT image. (a) iSCAT image of a GUV with 20 µm radius divided into 16 segments (2×2 µm²), each individually thresholded. (b) Segment-wise Fourier-transformed image. In each segment the distribution of the high-power frequencies can be approximated with an ellipse. (c) Raw iSCAT GUV image overlaid with red lines denoting vectors along the major ellipse axes each with a length determined by the ellipse eccentricity. The intersection of all vectors determines the coarse center of the GUV (red square).

To improve the accuracy, this center was used as the starting point for a second routine. Here, it was assumed that the path difference and the associated phase between the light reflected at the GUV surface and at the glass–water interface can be approximated with a parabola (1). In the parabolic approximation, the radial intensity distribution from the GUV rings is modulated quadratically as $I(r)=\cos(a r^2+\pi)$, where r is the radial distance from the GUV center in the recorded image, and a is a constant factor. Binning the average intensity values in intervals with quadratic spacing starting from the assumed GUV center therefore results in a periodicity with a frequency determined by Fourier transformation. The position $r=0$ for which the frequency has the maximum amplitude represents the GUV center.

The parabolic approximation is valid only in the small-angle regime, i.e. up to a relative phase of about 0.15 rad. For our experimental situation with a GUV radius typically between 10 and 30 µm, at

least 2.5 interference rings are present in this region, which is sufficient for finding the center with subpixel accuracy.

In the present example (Fig. S4a and b), we have plotted the average intensity versus the squared radial distance and the FT of the radial profile for a starting point ~3 pixel off the center (blue curve) and for the actual GUV center (red curve) in comparison. Although the routine for the coarse determination usually performs much better than 3 pixels deviation, this was chosen for illustration purposes and furthermore demonstrates that also in cases with a non-optimal starting point this routine performs well. In Fig. S4a it becomes clear that when the origin of the radial profile coincides with the actual GUV center, the periodicity is more pronounced and the corresponding peak frequency (marked with an arrow in Fig. S4b) has the maximum amplitude.

In Fig. S4c we have plotted the amplitude of the peak frequency around the initial center (in this case 3 pixels off) at (0,0). The distribution is smooth with only one global maximum, which represents the true center of the GUV. We determined this maximum iteratively using a MATLAB nonlinear optimization routine with a stopping criterion of 10^{-6} pixel accuracy.

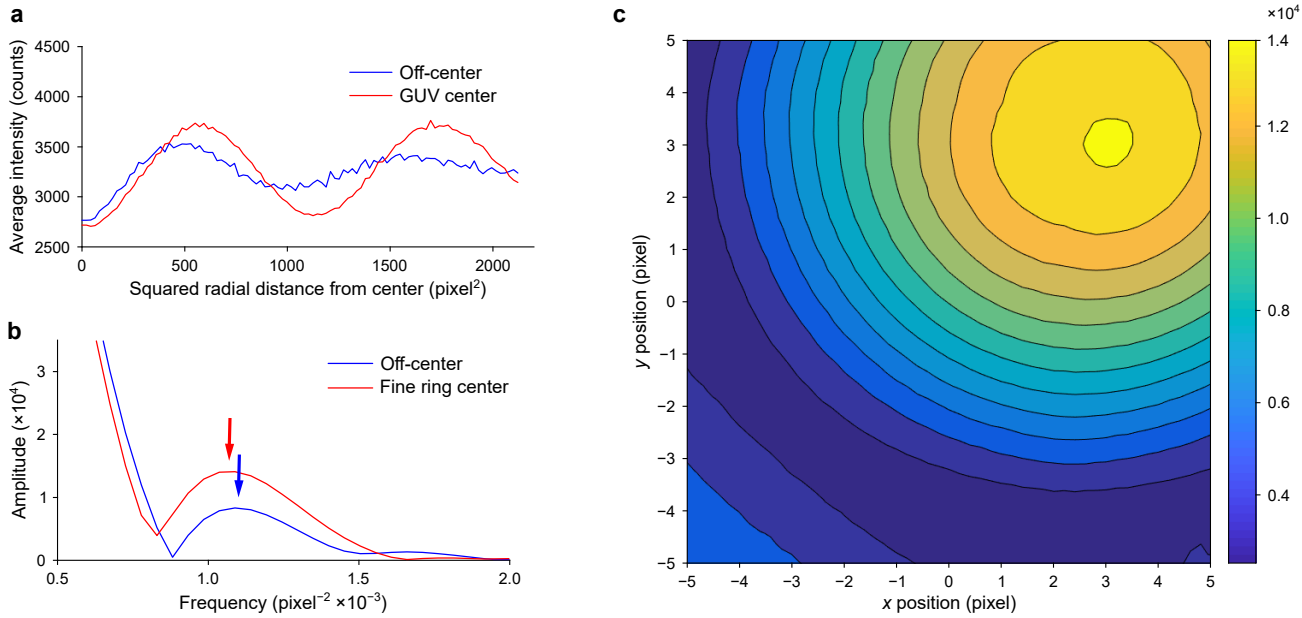

Figure S4 Fine determination of the GUV center position from its iSCAT image. (a) Average radial intensity profile of the GUV iSCAT image shown in Fig. S3c plotted against the quadratic distance from an assumed GUV center. For the true GUV center, the amplitude of the periodic intensity profile falls off much slower (red line) than for a radial profile with a center position about 3 pixels away from the GUV center (blue line). (b) Fourier transforms of the radial profiles shown in a) (with Hann window and zero padding). Note that the distance of 3 pixels used to calculate the off-center curves was chosen for illustration—the coarse determination routinely performs better than this. (c) Amplitude of the peak frequency from the Fourier transform as a function of the assumed GUV center position (with (0,0) corresponding to the coarsely determined position, in this case 3 pixels off). The position at which the amplitude is maximal corresponds to the fine GUV center position.

Unspecific attachment of liposomes on the GUV surface

To estimate the contribution of LUVs that are unspecifically interacting with GUVs (non SNARE-mediated interactions), we measured syb-LUV to GUV contact times (time from first contact that

appears as “docking” to “undocking”) in a situation where ΔN complex is either absent (protein free GUVs) or is inhibited by preincubation with a soluble syb fragment (1–96, for details see (2)). This was done using confocal time-lapse microscopy of LUVs labelled with membrane dye DiD and GUVs with dye DiI (both from Thermo Fisher Scientific) in the same way as described in (2). These measurements show that unspecific interactions of LUVs and GUVs arising from random collisions are short-lived, in our hands not exceeding 300 ms (Fig. S5).

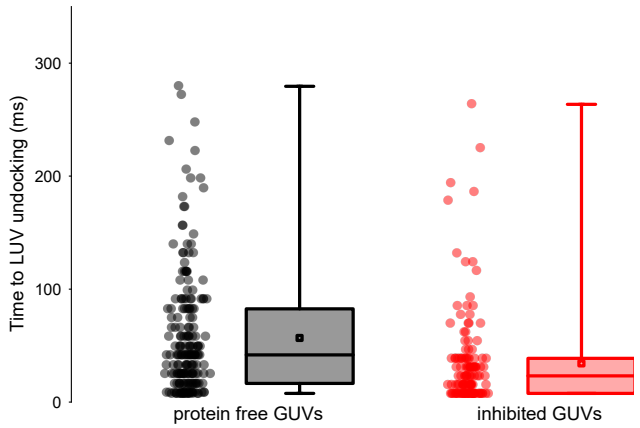

Figure S5 Prolonged docking of LUVs on GUV surface is SNARE specific. Syb WT-containing LUVs appear docked on protein free GUVs (black, N=209) or ΔN-GUVs preincubated with syb (1–96) (red, N=145) for only short periods of time, typically below 100 ms. Time from docking start to undocking was measured with time-lapse confocal microscopy (as in (2)). Boxes represent interquartile range, and whiskers below and above indicate full data range. Line in a box represents median and square point represents the mean.

Estimation of diffusional slowing down of LUVs induced by GUV proximity

In order to determine the effect of solvent and GUV proximity on the diffusion coefficient of freely diffusing LUVs, we employed a model of a vesicle moving parallel to a supported planar bilayer (3, 4). In this model diffusion coefficient $D_{\parallel}$:

$$D_{\parallel} = \frac{k_B T}{6 \pi \mu_s R} \times \beta_{\parallel}$$

is scaled with a $\beta_{\parallel}$ factor that describes increased hydrodynamic drag when particles diffuse parallel to a solid object:

$$\beta_{\parallel} = 1 - \frac{9}{16}\frac{R}{(R+h)} + \frac{1}{8}\left(\frac{R}{(R+h)}\right)^3 - \frac{45}{256}\left(\frac{R}{(R+h)}\right)^4 - \frac{1}{16}\left(\frac{R}{(R+h)}\right)^5$$

where R is the hydrodynamic radius of the vesicle and h is the separation distance between the vesicle and planar surface (GUV membrane in our case).

Diffusion coefficient and hydrodynamic radius of freely diffusing syb-LUVs (D_{free}) were measured in HEPES 20 mM (pH 7.4), KCl 150 mM buffer with dynamic light scattering (DynaPro Titan, Wyatt Technology) and were estimated to be 5.5 μm²/s and 44 nm, respectively. With these values diffusional slowing down of LUVs approaching GUV membrane could be estimated from the dependency (Fig. S6):

$$D_{\parallel} = D_{free} \times \beta_{\parallel}$$

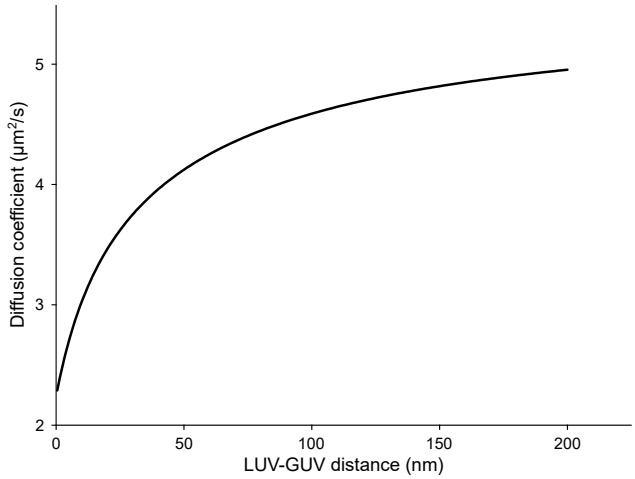

Figure S6 Diffusional slowing down of LUVs induced by GUV proximity. Estimation of decrease in a parallel diffusion coefficient of a free LUV approaching GUV according to model of (3, 4).

Effect of potential SNARE clustering on simulation of diffusion of loosely docked vesicles

As SNAREs might also diffuse in small clusters, we have investigated the effect of the SNARE cluster size on the diffusion coefficient of a loosely docked vesicle. Increasing number of SNAREs in a single tether does slightly slow down docked vesicles (compare black and red lines in Fig. S7), although much larger effects have number of independently diffusing tethers independent of number of proteins within the tether.

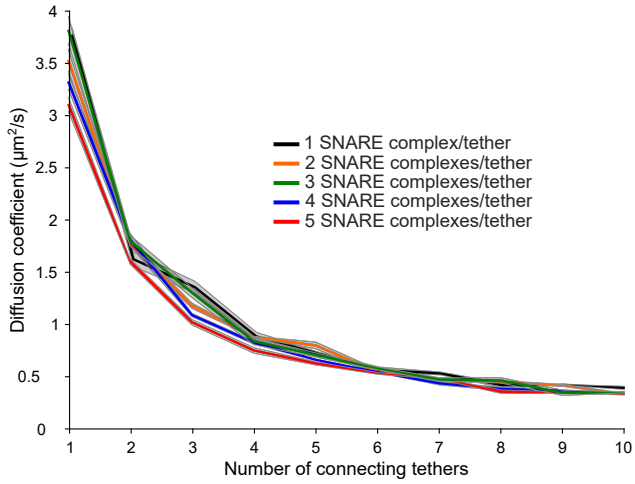

Figure S7 Dependence of loosely docked LUV's diffusion coefficient on the number of independent tethers and number of SNARE complexes contributing to each tether. The mean is represented by the thick line and the standard deviation of the mean is shown by the shaded area around it. Each diffusion coefficient was determined in 20 independent loose docking simulation runs. Diffusion coefficients of clustered SNAREs were obtained by estimating their hydrodynamic radius and calculating diffusion coefficient of a single cluster as in (5). Data for single SNARE complex as in Fig. 3e.

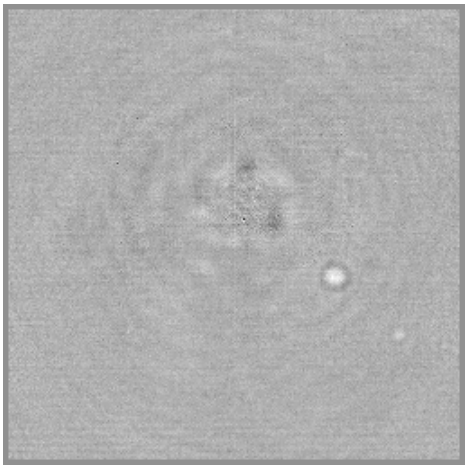

Movies 1–3 Vesicles docked and diffusing on a GUV surface. SITAR background-corrected iSCAT videos of a docked and diffusing AA syb-LUV (Movie 1), ∆84 syb-LUVs (Movie 2), and WT syb-LUVs (Movie 3) on a GUV. Frame rate = 1 kHz, recording time = 1s, videos slowed-down 20×, frame size = 16.28 µm × 16.28 µm.

Supporting References

1. Dobroiu, A., A. Alexandrescu, D. Apostol, V. Nascov, and V.S. Damian. 2000. Centering and profiling algorithm for processing Newton's rings fringe patterns. *OE*. 39:3201–3207.

2. Witkowska, A., and R. Jahn. 2017. Rapid SNARE-mediated fusion of liposomes and chromaffin granules with giant unilamellar vesicles. *Biophysical Journal*. 113:1251–1259.

3. Goldman, A.J., R.G. Cox, and H. Brenner. 1967. Slow viscous motion of a sphere parallel to a plane wall—I Motion through a quiescent fluid. *Chemical Engineering Science*. 22:637–651.

4. Kyoung, M., and E.D. Sheets. 2008. Vesicle diffusion close to a membrane: intermembrane interactions measured with fluorescence correlation spectroscopy. *Biophysical Journal*. 95:5789–5797.

5. Petrov, E.P., and P. Schwille. 2008. Translational Diffusion in Lipid Membranes beyond the Saffman-Delbrück Approximation. *Biophysical Journal*. 94:L41–L43.